ADHESIVE BEHAVIOR OF VERTICAL AND ANGLED POLYMER MICROFIBER ARRAYS

Michael P. Murphy, Burak Aksak, and Metin Sitti, Carnegie Mellon University, Pittsburgh, PA, USA, sitti@cmu.edu

Introduction

Biologically fibrillar dry adhesives found in insects and lizards allow repeatable controlled adhesion on a wide variety of surfaces by increasing the real area of contact [1]. This adhesion, called dry adhesion, is argued to arise from molecular surface forces such as van derWaals forces [1,2], possibly in combination with capillary forces [8,16]. The enhanced adhesion from fibrillar surfaces has been studied and described in terms of fracture mechanics, elastic beam theory, and surface interaction forces [3–5, 7, 9, 13, 14, 17], including analysis of the effects of tip shape and fiber size. Methods such as electron-beam lithography [6], micro/nanomolding [7, 10, 11, 15], and self-assembly are employed to fabricate fibers from polymers [2, 15], polymer organorods [12], and multi-walled carbon nanotubes [18, 19]. Whereas previous works focus mainly on either modeling or fabrication and testing of fibrillar interfaces only, this work aims to propose theoretical fibrillar interface models which are compared with the macroscale adhesion characterization results of fabricated microfibers to improve our understanding of the mechanics of dry microfibrillar adhesive interfaces. Detailed optical microscope images, mechanical behavior, and adhesion of micron scale fiber array interfaces during loading and unloading are shown in detail. 20-25 μm diameter polyurethane microfibers with different angle and aspect ratio are fabricated using ultra-violet (UV) lithography and polymer micromolding based fabrication technique and tested with a custom tensile macroscale adhesion measurement setup.

Adhesion Modeling

An analytical model for fiber adhesion is developed by combining the basic principles of elastic beam theory, surface interaction forces, and contact mechanics and applying them to high aspect ratio vertical and angled microfibers. The results from this model are compared to the adhesion experiments to determine the accuracy of the model and understand the adhesion mechanism of microfiber-surface interfaces in more depth.

There are two widely used parameters that quantify the adhesive properties of an interface: the maximum separation force and the energy dissipation. In this work, these parameters are modeled for a single fiber in contact with a surface, then this model is extended to arrays of fibers. For the single fiber analysis, the fiber geometry is taken as a cylindrical beam with a flat tip and small deflections. Equating the average tensile stress on the tip to the average adhesion strength (σ_c) the pull-off force (P_{cf}) is given by [20]

$$P_{cf} = \frac{3\pi a^3 \sigma_c}{\cos^2\theta(3a\cos\theta + 2L\sin\theta)} \quad (1)$$

where a is the fiber radius, L is the fiber length, and θ is the angle of the fiber to the normal of the surface.

Having determined the detachment criteria for a single fiber, it is possible to relate the deflection of the single fiber to the force it exerts on the surface through stiffness. Each fiber is assumed to be a linear spring with stiffness in the loading direction derived using the following assumptions; 1. Clamped-clamped boundary conditions; 2. The fiber tip is constrained to move only in the normal direction to the backing layer.

The relation between the deflection of the fiber and the force each fiber exerts on the surface (P_i) in contact can be summarized as follows:

$$P_i = \begin{cases} k\delta_i & -\delta_e \le \delta_i < \delta_{cr}/\cos\theta \quad (\textit{compressed or stretched}) \\ P_{cr}/\cos\theta & \delta_i \ge \delta_{cr}/\cos\theta \quad (\textit{buckled}) \\ 0 & \textit{otherwise} \quad (\textit{not attached}) \end{cases} \quad (2)$$

where k is the fiber stiffness in the normal direction, δ_i is the fiber deflection, $\delta_e = P_{cf}/k$ is the maximum fiber stretch before detachment, and P_{cr} and δ_{cr} are the critical buckling force and deflection, respectively. The overall energy required to separate the fiber from the surface is [9]

$$u_d = \omega\pi a^2 + \tfrac{1}{2}k^2\delta_e \quad (3)$$

where ω is the work of adhesion.

The adhesion behavior of an array of fibers can be characterized by summing the force contributions of each individual fiber using the conditions in (2). The deflection of each fiber (δ_i) is determined by the surface roughness parameters and the relative displacement (Δ) of the two surfaces as in Fig.1.

The surface used in the experiments and simulations is a hemisphere (Fig. 1) because a hemisphere represents a special case of a rough surface with a well-defined height distribution which is immune to alignment and orientation issues. The radius of the sphere is chosen to be much larger then the fiber radius so that the local flat contact assumption applies.

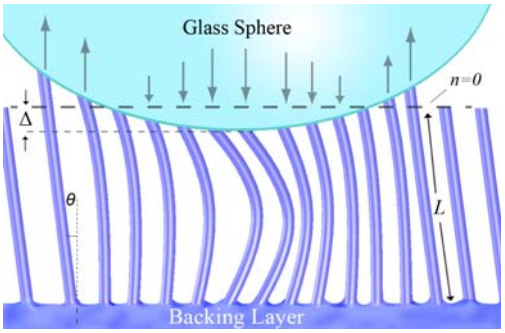

Figure 1. Schematic of a sphere retracting from an array of fibers. The fibers in the middle of the sphere are compressed, the ones that are in contact on the edges are stretched. The arrows show the direction and relative magnitude of the forces on the fibers.

Microfiber Fabrication

Polymer microfiber arrays are fabricated through a micromolding process which duplicates lithographically formed master template structures with a desired fiber material. This technique enables fabrication of fiber array patches on up to an 8 inch wafer inexpensively and with high yields. This is a significant advantage with compared to other proposed fibrillar adhesive fabrication techniques [6], [12], [19].

First, a master template is fabricated on a glass wafer using standard UV photolithography and SU-8 photoresist. By angling the wafer during exposure, fibers with non-vertical orientation can be formed. Fabrication details are described in previous work [20].

Large arrays on the order of 300 mm^2 of high aspect ratio independent fibers are created. Fibers with diameters from 4 to 25 μm are produced with aspect ratios of up to 20:1. 10:1 aspect ratio fiber arrays exhibit excellent uniformity and tend to remain upright.

The master template wafer is molded with a silicone rubber (HS-II, Dow Corning) and carefully peeled away to form a compliant negative mold. This mold is then used to vacuum mold polyurethanes or other curable materials into the master template fiber geometry. Using this method, the microfiber material can be chosen to suit the intended design.

Experiments and Results

Fiber array test samples were fabricated with a polyurethane elastomer (ST-1060; BJB Enterprises) which has high tensile strength (6 MPa). The hardness of the polymer is Shore 60A, and was determined through tensile testing to have Young's modulus of approximately 2.9 MPa. Fiber arrays with varied lengths and angles were fabricated for testing as described in Table 1. These geometries were selected because they allow consistent fabrication results and are large enough to be easily visible with optical microscopy. The backing layer is approximately 2.5 mm for all samples.

Table 1. Fiber sample geometry

Sample Type	Height (μm)	Diameter (μm)	Length (μm)	Angle (°)
Short Vertical	48	20	48	0
Long Vertical	100	25	100	0
Long Angled	75	25	79	18

The custom macroscale adhesion measurement system consists of a top-view reflection type optical microscope (Nikon Eclipse L200) or an inverted optical microscope (Nikon Eclipse TE200) with an automated high precision stage (MFA-CC; Newport) which holds a high resolution load cell (GSO-25; Transducer Techniques Inc.). A hemispherical 12 mm diameter glass hemisphere (QUHS- 12; ISP Optics) is connected to the load cell. The adhesive samples are placed on the microscope stage with the fiber arrays facing toward the glass hemisphere. Custom real-time software controls the stage to move the hemisphere into contact with the fiber sample at a fixed velocity until a pre-specified preload force is reached. The hemisphere is then quasi-statically retracted at a speed of 1 μm/s until it detaches from the sample. The software continually captures the force data from the load cell as well as timestamped video from the microscope.

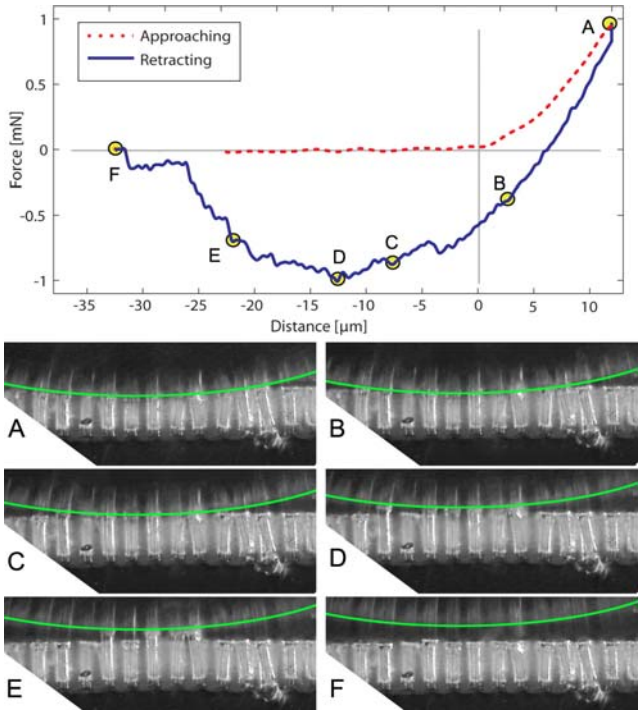

Figure 2. Sample force-distance experimental data and corresponding video images. Curved lines overlayed for clarity.

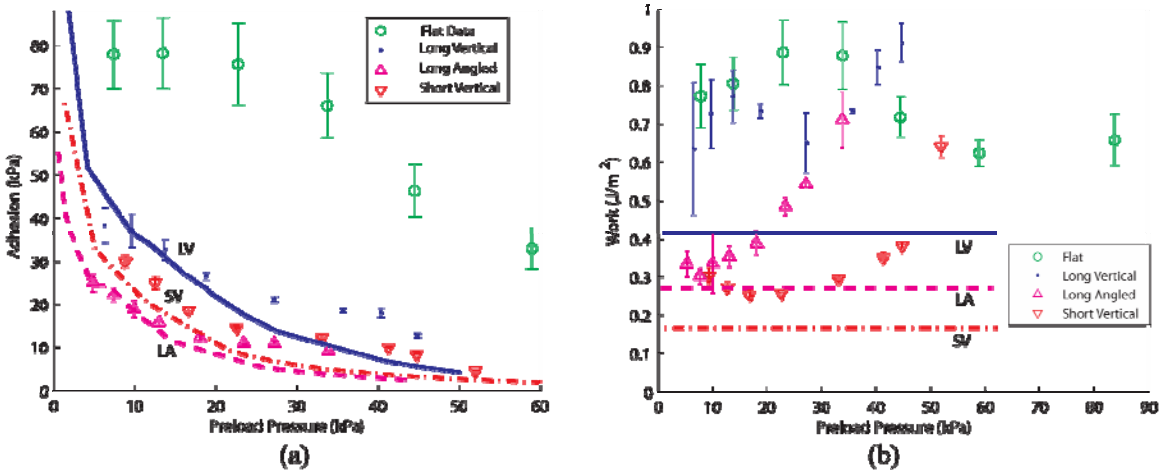

Figure 3. Adhesion pressure (a) and overall work of adhesion (b) as a function of preload. The simulation results are lines (LV: long vertical, LA: long angled, SV: short vertical) and the experimental data are markers.

For computing the overall work of adhesion for the macroscale measurements on the fiber arrays, force-distance data from the hemisphere tests are used to calculate the energy dissipation U_d by numerically integrating the area between the loading and unloading force curves. Force-distance data from a single measurement is shown in Figure 2. In this case, an array of long vertical ST-1060 fibers was tested with a 1 mm diameter steel sphere. The force during the approach is zero until the sphere makes initial contact with the fibers at $n=0$. The preload force (P_p) is the maximum positive force peak (A) when the sphere has penetrated the fiber array by distance Δ_p. While the hemisphere is retracting the force increases as more fibers are stretched (B-D). The maximum separation force (P_a) is the value of the negative peak (D) where the sum of the forces of the contacting fibers is the greatest. After this point, the total force decreases because the loss in adhesion force due to fibers detaching is greater than the increase in force due to the extension of the attached fibers (E). Finally, the last fiber is stretched to its maximum ($\Delta_e = \delta_e$) and then pulls off, returning the overall force to zero (F).

A series of experiments were conducted with the glass hemisphere where the preload force was varied from 1 to 50 mN, and the approach and retraction speeds were 1 μm/s. Five measurements were taken for each sample at each of eight pre-selected preload values, and the contact point was moved to a different location on the fiber array for each measurement.

The equations from modeling section were implemented in a MATLAB® simulation, in which the parameters from the experiment were used to predict the adhesion of the fiber arrays. The results are compared to the experimental data in Figure 3. Figure 3 demonstrate a general agreement between the numerical simulations and the data for the fiber samples. The adhesion pressures are predicted with high accuracy whereas the work of adhesion is much higher than predicted possibly due to unmodeled behavior such as deflection of the compliant backing layer.

Conclusions

A model was developed to predict the adhesive properties of arrays of microfibers based on fiber bending, compression, buckling and extension in combination with contact mechanics. The model takes into account parameters such as fiber material properties, fiber dimensions, fiber angle, and surface geometry. Also, the feasibility of fabricating high density and high aspect ratio microfiber arrays in large areas has been confirmed. The use of UV photolithography as a fabrication process for high aspect ratio self-supporting microfibers has been demonstrated, including fabrication of angled fiber arrays. Micromolding high aspect ratio angled polymer microfiber arrays by means of a compliant intermediate mold was demonstrated. Fabricated microfiber array samples were tested using a custom adhesion measurement system and the results were compared with theory. The simulation results were found to predict the macroscale adhesive behavior of the microfiber arrays.

References

1. K. Autumn *et al*., Nature, 2000, 405:681–685.
2. K. Autumn, *et al,*. PNAS, 2002, 99:12252–56.
3. J. Y. Chung and M. K. Chaudhury, J. R. Soc. Interface, 2005, 2:55–61.
4. A. Crosby *et al.*, Langmuir, 2005, 21:11738–11743.
5. H. Gao and H. Yao. PNAS, 2004, 101(21):7851–7856.
6. A. K. Geim *et al.* Nature Materials, 2003, 2:461 – 463.
7. N. J. Glassmaker *et al.*, J. R. Soc. Interface, 2004, 23–33.
8. G. Huber *et al.* PNAS, 2005, 102:16293–16296.
9. C. Hui *et al*. J. R. Soc. Interface, 2004, 1:35 – 48.
10. C. Majidi *et al*. IMECE, 2004, 579–584.
11. C. Menon, *et al*. ROBIO, 2004, 431–436.
12. M. T. Northen and K. L. Turner. Nanotechnology, 2005, 16:1159–1166.
13. B. N. J. Perrson and S. Gorb., Journal of Chemical Physics, 2003,119 (21)11437–11444.
14. B. N. J. Persson. Journal of Chemical Physics, 2003, 118:7614–7621
15. M. Sitti and R. Fearing. JAST, 2003 17(5):1055–74.
16. W. Sun *et al.* Biophysical Journal: Biophysical Letters, L14–L17, 2005.
17. T. Tang *et al*. Journal of The Royal Society, Interface, 2005, 2(5):505 – 516.
18. B. Yurdumakan *et al.* Chemical Communications, 2005, page 3799-3801.
19. Y. Zhao *et al.* Journal of Vacuum Science & Technology B: Microelectronics and Nanometer Structures, 2006, 24:331–335.
20. B. Aksak *et al.* Langmuir, 2007, (in review).